



*Discrete Ordinates Radiation Transport using
Higher-Order Finite Element Spatial Discretizations
on Meshes with Curved Surfaces*

Dissertation Defense

Douglas N. Woods

4 June 2018

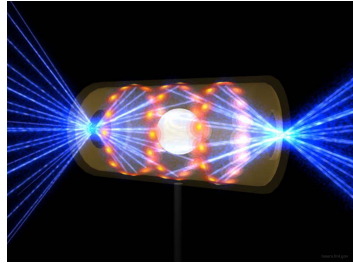
Outline

- Introduction
- Objectives
- Methods
- MIP DSA
 - Implementation
 - Numerical Results
- *R-Z* Geometry
 - Implementation
 - Numerical Results
- Conclusions

Introduction

Radiation-hydrodynamics

- High energy density physics
 - astrophysics
 - inertial confinement fusion

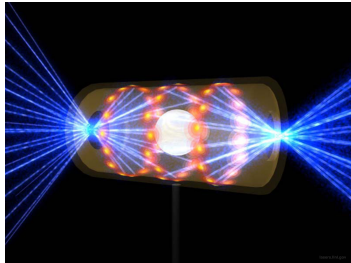


<https://lasers.llnl.gov/content/assets/images/media/photo-gallery/large/nif-1209-18059.jpg>

Introduction

Radiation-hydrodynamics

- High energy density physics
 - astrophysics
 - inertial confinement fusion
- Blackbody radiation can influence the energy, temperature, momentum, pressure of the fluid

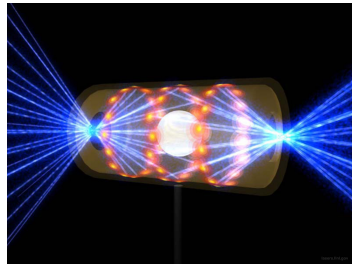


<https://lasers.llnl.gov/content/assets/images/media/photo-gallery/large/nif-1209-18059.jpg>

Introduction

Radiation-hydrodynamics

- High energy density physics
 - astrophysics
 - inertial confinement fusion
- Blackbody radiation can influence the energy, temperature, momentum, pressure of the fluid
- Radiation-hydrodynamics to study these problems

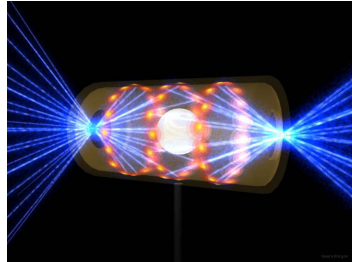


<https://lasers.llnl.gov/content/assets/images/media/photo-gallery/large/nif-1209-18059.jpg>

Introduction

Radiation-hydrodynamics

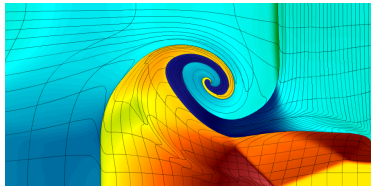
- High energy density physics
 - astrophysics
 - inertial confinement fusion
- Blackbody radiation can influence the energy, temperature, momentum, pressure of the fluid
- Radiation-hydrodynamics to study these problems
- Can study radiation transport and hydrodynamics separately



<https://lasers.llnl.gov/content/assets/images/media/photo-gallery/large/nif-1209-18059.jpg>

Introduction

BLAST — LLNL ALE hydrodynamics code



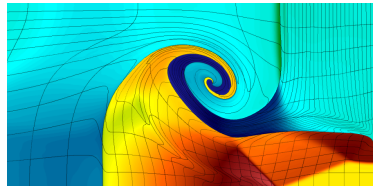
multi-material shock hydrodynamics problem solved with BLAST: 8th-order kinematics, 7th-order thermodynamics

<https://computation.llnl.gov/project/blast/>

- High-order (HO) finite element spatial discretization

Introduction

BLAST — LLNL ALE hydrodynamics code



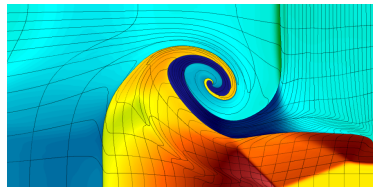
multi-material shock hydrodynamics problem solved with BLAST: 8th-order kinematics, 7th-order thermodynamics

<https://computation.llnl.gov/project/blast/>

- High-order (HO) finite element spatial discretization
- Meshes with curved surfaces
 - Straight-edged meshes restrict the accuracy of the compressible Euler equations
 - “Essential for higher-order accuracy”

Introduction

BLAST — LLNL ALE hydrodynamics code



multi-material shock hydrodynamics problem solved with BLAST: 8th-order kinematics, 7th-order thermodynamics

<https://computation.llnl.gov/project/blast/>

- High-order (HO) finite element spatial discretization
- Meshes with curved surfaces
 - Straight-edged meshes restrict the accuracy of the compressible Euler equations
 - “Essential for higher-order accuracy”
- More accurately model:
 - Fluid flow geometry in Lagrangian framework with curved meshes
 - Can model a shock front within a single zone - higher resolution
 - Radial flow symmetry

Introduction

High-order radiation transport

- HO ($p \geq 2$) S_N transport FEM research is relatively new 
- FEM approximates a polynomial solution
- Low-order (LO) ($p = 1$) methods are less computationally expensive
- Expected spatial convergence of $O(p + 1)$ have been shown
- HO DFEMs are accurate in the diffusion limit
- Some HO DFEM research in 1-D thermal radiation transport

Introduction

High-order radiation transport

- HO ($p \geq 2$) S_N transport FEM research is relatively new
 - FEM approximates a polynomial solution
 - Low-order (LO) ($p = 1$) methods are less computationally expensive
 - Expected spatial convergence of $O(p + 1)$ have been shown
 - HO DFEMs are accurate in the diffusion limit
 - Some HO DFEM research in 1-D thermal radiation transport
- R-Z geometry has only been developed using LO finite elements
 - 2nd-order spatial convergence for linear methods (BLD, PWLD, etc.)
 - Accurate in the diffusion limit



Introduction

High-order radiation transport

- HO ($p \geq 2$) S_N transport FEM research is relatively new
 - FEM approximates a polynomial solution
 - Low-order (LO) ($p = 1$) methods are less computationally expensive
 - Expected spatial convergence of $O(p + 1)$ have been shown
 - HO DFEMs are accurate in the diffusion limit
 - Some HO DFEM research in 1-D thermal radiation transport
- R-Z geometry has only been developed using LO finite elements
 - 2nd-order spatial convergence for linear methods (BLD, PWLD, etc.)
 - Accurate in the diffusion limit
- Structured/unstructured quadrilateral and triangular meshes
 - Some research for meshes with curved surfaces
 - Do not degrade $O(p + 1)$ spatial convergence rate

Objectives

- Use MFEM, a general finite element library (mfem.org):
 1. Modified interior penalty (MIP) diffusion synthetic acceleration (DSA)
 - Implement MIP DSA equations using homogeneous Robin (i.e. vacuum) boundary conditions
 - Examine and compare spectral radii to MIP DSA using homogeneous Dirichlet boundary conditions

Objectives

- Use MFEM, a general finite element library (mfem.org):
 1. Modified interior penalty (MIP) diffusion synthetic acceleration (DSA)
 - Implement MIP DSA equations using homogeneous Robin (i.e. vacuum) boundary conditions
 - Examine and compare spectral radii to MIP DSA using homogeneous Dirichlet boundary conditions
 2. R - Z geometry 
 - Numerically solve HO S_N transport equation on meshes with curved surfaces
 - Preserve 1-D spherical symmetry

Methods

HO DGFEM spatial discretization

- Steady-state, monoenergetic radiation transport equation

$$\begin{aligned}\Omega_m \cdot \nabla \psi_m + \sigma_t \psi_m &= \frac{1}{4\pi} \sigma_s \phi + \frac{1}{4\pi} S_0 \\ \phi &= \sum_m w_m \psi_m\end{aligned}$$

Methods

HO DGFEM spatial discretization

- Steady-state, monoenergetic radiation transport equation

$$\Omega_m \cdot \nabla \psi_m + \sigma_t \psi_m = \frac{1}{4\pi} \sigma_s \phi + \frac{1}{4\pi} S_0$$
$$\phi = \sum_m w_m \psi_m$$



- Standard discontinuous Galerkin finite element method (DGFEM) spatial discretization

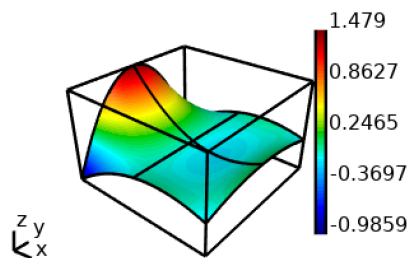
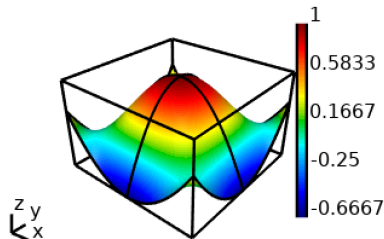
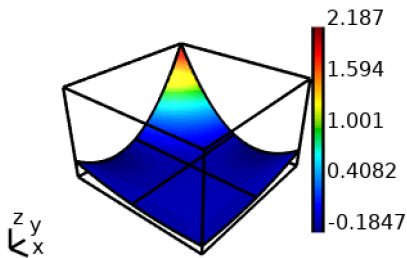
$$(\Omega_m \cdot \nabla \psi_m, v_i)_{\mathcal{D}_k} + (\sigma_t \psi_m, v_i)_{\mathcal{D}_k} = \frac{1}{4\pi} (\sigma_s \phi, v_i)_{\mathcal{D}_k} + \frac{1}{4\pi} (S_0, v_i)_{\mathcal{D}_k}$$

$$\psi(\mathbf{x}, \Omega_m) \approx \sum_j b_j(\mathbf{x}) \psi_j(\Omega_m)$$



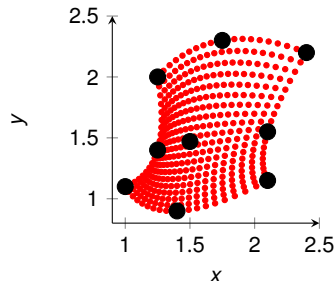
Methods

HO DGFEM basis functions allow for more complex solution shapes

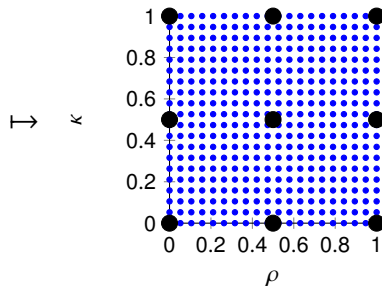


Methods

HO mapping allows for meshes with curved surfaces



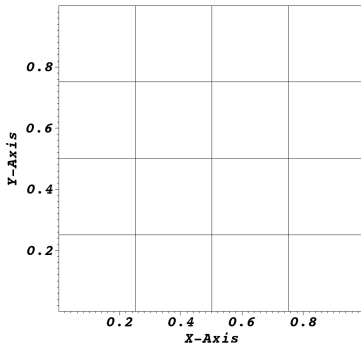
Physical element



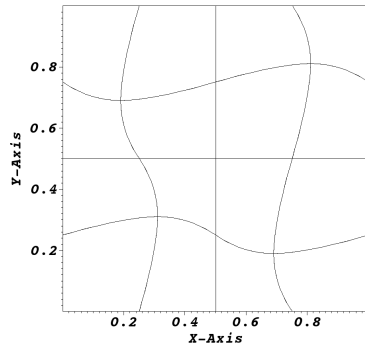
Reference element

Methods

HO mesh transformation example



Orthogonal mesh



3rd-order mesh

Methods

Create DGFEM matrices using MFEM, solve using a direct solver

- MFEM generates local matrices and vectors for a variety of operators, assembles them into global linear algebra system
 - High-order finite elements
 - Create and transform meshes with curved surfaces

Methods

Create DGFEM matrices using MFEM, solve using a direct solver

- MFEM generates local matrices and vectors for a variety of operators, assembles them into global linear algebra system
 - High-order finite elements
 - Create and transform meshes with curved surfaces
- Solve linear system directly with UMFPack
(<http://faculty.cse.tamu.edu/davis/suitesparse.html>)
- Visualize solutions with VisIt
(<https://wci.llnl.gov/simulation/computer-codes/visit>)

Diffusion Synthetic Acceleration

Source iteration acceleration

- Source iteration to solve radiation transport equation
 - Iterate on scalar flux until scattering source converges
 - Can converge arbitrarily slowly with increased scattering

$$\Omega \cdot \nabla \psi_m^{(\ell+1)} + \sigma_t \psi_m^{(\ell+1)} = \frac{1}{4\pi} \sigma_s \phi^{(\ell)} + \frac{1}{4\pi} S_0$$

$$\phi^{(\ell+1)} = \sum_m w_m \psi_m^{(\ell+1)}$$



Diffusion Synthetic Acceleration

Source iteration acceleration

- Source iteration to solve radiation transport equation
 - Iterate on scalar flux until scattering source converges
 - Can converge arbitrarily slowly with increased scattering

$$\Omega \cdot \nabla \psi_m^{(\ell+1)} + \sigma_t \psi_m^{(\ell+1)} = \frac{1}{4\pi} \sigma_s \phi^{(\ell)} + \frac{1}{4\pi} S_0$$

$$\phi^{(\ell+1)} = \sum_m w_m \psi_m^{(\ell+1)}$$

- Source iteration acceleration
 - Solve diffusion equation to make a small “correction” to the radiation transport solution

Diffusion Synthetic Acceleration

DSA algorithm

- Diffusion synthetic acceleration (DSA) algorithm

$$\Omega \cdot \nabla \psi_m^{(\ell+1/2)} + \sigma_t \psi_m^{(\ell+1/2)} = \frac{1}{4\pi} \sigma_s \phi^{(\ell)} + \frac{1}{4\pi} S_0$$
$$\phi^{(\ell+1/2)} = \sum_{m=1}^M w_m \psi_m^{(\ell+1/2)}$$

Diffusion Synthetic Acceleration

DSA algorithm

- Diffusion synthetic acceleration (DSA) algorithm

$$\Omega \cdot \nabla \psi_m^{(\ell+1/2)} + \sigma_t \psi_m^{(\ell+1/2)} = \frac{1}{4\pi} \sigma_s \phi^{(\ell)} + \frac{1}{4\pi} S_0$$

$$\phi^{(\ell+1/2)} = \sum_{m=1}^M w_m \psi_m^{(\ell+1/2)}$$

$$-\nabla \cdot D \nabla \varphi^{(\ell+1/2)} + \sigma_a \varphi^{(\ell+1/2)} = \sigma_s (\phi^{(\ell+1/2)} - \phi^{(\ell)})$$



Diffusion Synthetic Acceleration

DSA algorithm

- Diffusion synthetic acceleration (DSA) algorithm

$$\Omega \cdot \nabla \psi_m^{(\ell+1/2)} + \sigma_t \psi_m^{(\ell+1/2)} = \frac{1}{4\pi} \sigma_s \phi^{(\ell)} + \frac{1}{4\pi} S_0$$

$$\phi^{(\ell+1/2)} = \sum_{m=1}^M w_m \psi_m^{(\ell+1/2)}$$

$$-\nabla \cdot D \nabla \varphi^{(\ell+1/2)} + \sigma_a \varphi^{(\ell+1/2)} = \sigma_s (\phi^{(\ell+1/2)} - \phi^{(\ell)})$$

$$\phi^{(\ell+1)} = \phi^{(\ell+1/2)} + \varphi^{(\ell+1/2)}$$



Modified Interior Penalty DSA

Implemented with homogeneous Dirichlet boundary conditions

- Wang and Ragusa (2010) derived modified interior penalty (MIP) DSA with homogeneous Dirichlet boundary conditions

Modified Interior Penalty DSA

Implemented with homogeneous Dirichlet boundary conditions

- Wang and Ragusa (2010) derived modified interior penalty (MIP) DSA with homogeneous Dirichlet boundary conditions
- Bilinear form:

$$\begin{aligned} b_{MIP,D}(\varphi, v) = & (\sigma_a \varphi, v)_D + (D \nabla \varphi, \nabla v)_D \\ & + (\kappa_e [\![\varphi]\!], [\![v]\!])_{\partial D^i} + ([\![\varphi]\!], \{D \partial_n v\})_{\partial D^i} + (\{D \partial_n \varphi\}, [\![v]\!])_{\partial D^i} \\ & + (\kappa_e \varphi, v)_{\partial D^d} - \frac{1}{2} (\varphi, D \partial_n v)_{\partial D^d} - \frac{1}{2} (D \partial_n \varphi, v)_{\partial D^d} \end{aligned}$$

Modified Interior Penalty DSA

Implemented with homogeneous Dirichlet boundary conditions

- Wang and Ragusa (2010) derived modified interior penalty (MIP) DSA with homogeneous Dirichlet boundary conditions
- Bilinear form:

$$\begin{aligned} b_{MIP,D}(\varphi, v) = & (\sigma_a \varphi, v)_D + (D \nabla \varphi, \nabla v)_D \\ & + (\kappa_e [\![\varphi]\!], [\![v]\!])_{\partial D^i} + ([\![\varphi]\!], \{D \partial_n v\})_{\partial D^i} + (\{D \partial_n \varphi\}, [\![v]\!])_{\partial D^i} \\ & + (\kappa_e \varphi, v)_{\partial D^d} - \frac{1}{2} (\varphi, D \partial_n v)_{\partial D^d} - \frac{1}{2} (D \partial_n \varphi, v)_{\partial D^d} \end{aligned}$$

- Linear form:

$$\ell_{MIP}(v) = \left(\sigma_s [\phi^{(\ell+1/2)} - \phi^{(\ell)}], v \right)_D$$

Modified Interior Penalty DSA

Stabilization parameter is a function of an arbitrary coefficient

- “Switch” within the stabilization parameter between diffusion conforming form (DCF) and interior penalty (IP) method

$$\kappa_e = \max\left(\kappa_e^{IP}, \frac{1}{4}\right)$$

Modified Interior Penalty DSA

Stabilization parameter is a function of an arbitrary coefficient

- “Switch” within the stabilization parameter between diffusion conforming form (DCF) and interior penalty (IP) method

$$\kappa_e = \max\left(\kappa_e^{IP}, \frac{1}{4}\right)$$

$$\kappa_e^{IP} = \begin{cases} \frac{c(p^+)}{2} \frac{D^+}{h_\perp^+} + \frac{c(p^-)}{2} \frac{D^-}{h_\perp^-}, & \text{on interior edges} \\ c(p) \frac{D}{h_\perp}, & \text{on boundary edges} \end{cases}$$

Modified Interior Penalty DSA

Stabilization parameter is a function of an arbitrary coefficient

- “Switch” within the stabilization parameter between diffusion conforming form (DCF) and interior penalty (IP) method

$$\kappa_e = \max\left(\kappa_e^{IP}, \frac{1}{4}\right)$$

$$\kappa_e^{IP} = \begin{cases} \frac{c(p^+)}{2} \frac{D^+}{h_\perp^+} + \frac{c(p^-)}{2} \frac{D^-}{h_\perp^-}, & \text{on interior edges} \\ c(p) \frac{D}{h_\perp}, & \text{on boundary edges} \end{cases}$$

$$c(p) = C p(p+1)$$

Modified Interior Penalty DSA

Stabilization parameter is a function of an arbitrary coefficient

- “Switch” within the stabilization parameter between diffusion conforming form (DCF) and interior penalty (IP) method

$$\kappa_e = \max\left(\kappa_e^{IP}, \frac{1}{4}\right)$$

$$\kappa_e^{IP} = \begin{cases} \frac{c(p^+)}{2} \frac{D^+}{h_\perp^+} + \frac{c(p^-)}{2} \frac{D^-}{h_\perp^-}, & \text{on interior edges} \\ c(p) \frac{D}{h_\perp}, & \text{on boundary edges} \end{cases}$$

$$c(p) = \textcolor{blue}{C} p(p+1)$$

- $\textcolor{blue}{C}$ is an arbitrary constant (i.e. 2, 4, 6)

Modified Interior Penalty DSA

Implemented with homogeneous Robin boundary conditions

- We modify the MIP DSA equations to include homogeneous Robin boundary conditions
 - Dirichlet BC fixes boundary solution to $\varphi = 0$
 - Robin BC is a true vacuum boundary condition
- Implement the boundary condition:

$$0 = \frac{1}{4}\varphi + \frac{1}{2}D\boldsymbol{\nabla}\varphi \cdot \hat{\mathbf{n}}$$

Modified Interior Penalty DSA

Implemented with homogeneous Robin boundary conditions

- We modify the MIP DSA equations to include homogeneous Robin boundary conditions
 - Dirichlet BC fixes boundary solution to $\varphi = 0$
 - Robin BC is a true vacuum boundary condition
- Implement the boundary condition:

$$0 = \frac{1}{4}\varphi + \frac{1}{2}D\boldsymbol{\nabla}\varphi \cdot \hat{n}$$

$$-(\boldsymbol{\nabla} \cdot D\boldsymbol{\nabla}\varphi, v)_{\mathcal{D}} = (D\boldsymbol{\nabla}\varphi, \boldsymbol{\nabla}v)_{\mathcal{D}} - (D\boldsymbol{\nabla}\varphi \cdot \hat{n}, v)_{\partial\mathcal{D}}$$

Modified Interior Penalty DSA

Implemented with homogeneous Robin boundary conditions

- We modify the MIP DSA equations to include homogeneous Robin boundary conditions
 - Dirichlet BC fixes boundary solution to $\varphi = 0$
 - Robin BC is a true vacuum boundary condition
- Implement the boundary condition:

$$0 = \frac{1}{4}\varphi + \frac{1}{2}D\boldsymbol{\nabla}\varphi \cdot \hat{n}$$

$$-(\boldsymbol{\nabla} \cdot D\boldsymbol{\nabla}\varphi, v)_{\mathcal{D}} = (D\boldsymbol{\nabla}\varphi, \boldsymbol{\nabla}v)_{\mathcal{D}} - (D\boldsymbol{\nabla}\varphi \cdot \hat{n}, v)_{\partial\mathcal{D}}$$

$$-(\boldsymbol{\nabla} \cdot D\boldsymbol{\nabla}\varphi, v)_{\mathcal{D}} = (D\boldsymbol{\nabla}\varphi, \boldsymbol{\nabla}v)_{\mathcal{D}} - (D\boldsymbol{\nabla}\varphi \cdot \hat{n}, v)_{\partial\mathcal{D}^i} - (D\boldsymbol{\nabla}\varphi \cdot \hat{n}, v)_{\partial\mathcal{D}^d}$$



Modified Interior Penalty DSA

Implemented with homogeneous Robin boundary conditions

- We modify the MIP DSA equations to include homogeneous Robin boundary conditions
 - Dirichlet BC fixes boundary solution to $\varphi = 0$
 - Robin BC is a true vacuum boundary condition
- Implement the boundary condition:

$$0 = \frac{1}{4}\varphi + \frac{1}{2}D\boldsymbol{\nabla}\varphi \cdot \hat{n}$$

- Bilinear form:

$$\begin{aligned} b_{MIP,R}(\varphi, v) &= (\sigma_a \varphi, v)_{\mathcal{D}} + (D \boldsymbol{\nabla}\varphi, \boldsymbol{\nabla}v)_{\mathcal{D}} \\ &+ (\kappa_e [\![\varphi]\!], [\![v]\!])_{\partial\mathcal{D}^i} + ([\![\varphi]\!], \{D \partial_n v\})_{\partial\mathcal{D}^i} + (\{D \partial_n \varphi\}, [\![v]\!])_{\partial\mathcal{D}^i} \\ &+ \left(\frac{1}{2}\varphi, v \right)_{\partial\mathcal{D}^d} \end{aligned}$$



MIP DSA Sensitivity Study

Sensitivity of spectral radius to element order p , constant C , DSA boundary condition

- Wang and Ragusa studied convergence rates of their MIP DSA formulation
- Sensitivity studies on the spectral radius for
 - Finite element order p
 - Varying the constant C (part of the stabilization parameter κ_e) of the MIP DSA equations
 - Homogeneous Dirichlet versus Robin boundary conditions

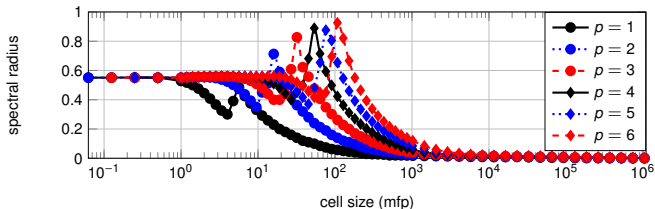
MIP DSA Sensitivity Study

Sensitivity of spectral radius to element order p , constant C , DSA boundary condition

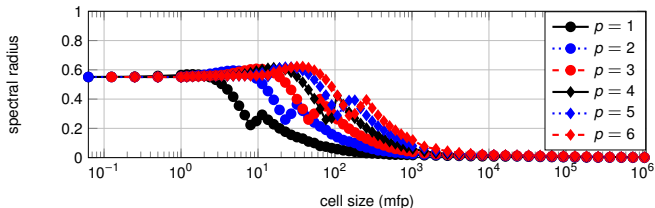
- Wang and Ragusa studied convergence rates of their MIP DSA formulation
- Sensitivity studies on the spectral radius for
 - Finite element order p
 - Varying the constant C (part of the stabilization parameter κ_e) of the MIP DSA equations
 - Homogeneous Dirichlet versus Robin boundary conditions
- Problem description:
 - 10x10 mesh on unit square
 - Vacuum boundaries
 - Scattering ratio $c = 0.9999$
 - Total cross section σ_t selected at run time to establish cell size

MIP DSA Sensitivity Study

Unconditionally converges with homogeneous Dirichlet boundary conditions



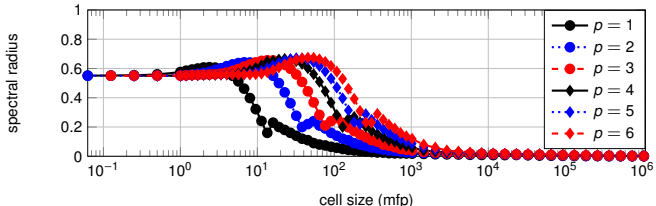
Spectral radius data for varying p with $C = 2$.



Spectral radius data for varying p with $C = 4$.

MIP DSA Sensitivity Study

Unconditionally converges with homogeneous Dirichlet boundary conditions



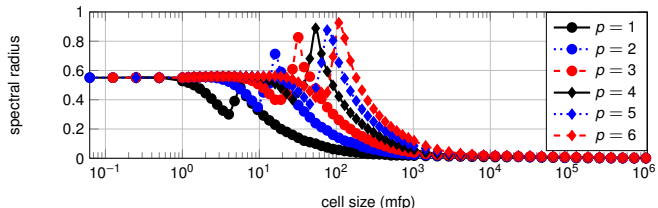
Spectral radius data for varying p with $C = 6$.



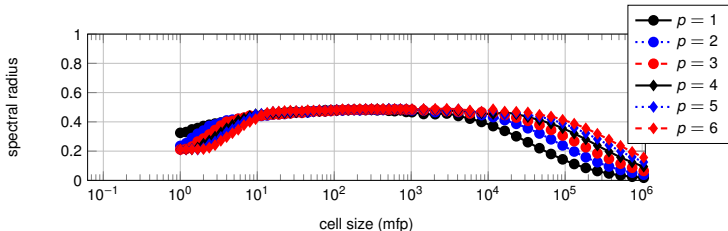
- Our $C = 2$ results resemble Wang and Ragusa's results
- Unconditionally converging ($\rho < 1$)
- Substantial dependence on C and p
- Orthogonal and 3rd-order meshes exhibit similar behavior

MIP DSA Sensitivity Study

Unconditionally converges with homogeneous Robin boundary conditions



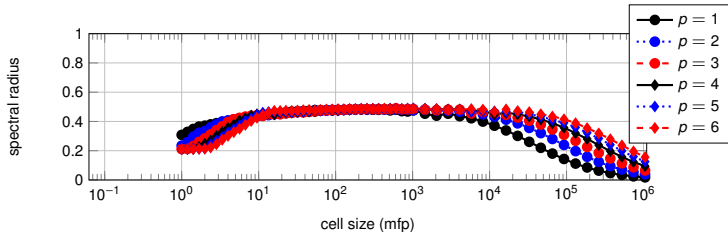
Spectral radius data for varying p with $C = 2$ (Dirichlet BC repeated).



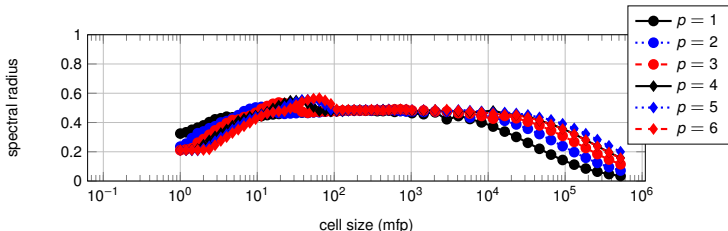
Spectral radius data for varying p with $C = 2$.

MIP DSA Sensitivity Study

Unconditionally converges with homogeneous Robin boundary conditions



Spectral radius data for varying p with $C = 4$.



Spectral radius data for varying p with $C = 6$.

MIP DSA Sensitivity Study

Unconditionally converges with homogeneous Robin boundary conditions

- Unconditionally convergent ($\rho < 1$)
- Much less dependence on C and p
- Intermediate optical thickness has a smoother profile than Dirichlet boundary conditions
- Optically thick regime converges slower than Dirichlet boundary conditions



R-Z Geometry

Streaming term introduces an angular derivative

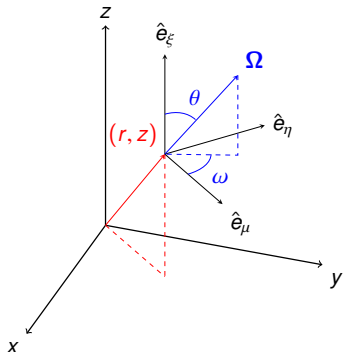
$$\frac{\mu}{r} \frac{\partial}{\partial r} (r \psi) + \xi \frac{\partial}{\partial z} \psi - \frac{1}{r} \frac{\partial}{\partial \omega} (\eta \psi) + \sigma_t \psi = \frac{1}{2\pi} \sigma_s \phi + \frac{1}{2\pi} S_0$$

$$\mu = \sqrt{1 - \xi^2} \cos(\omega)$$

$$\eta = \sqrt{1 - \xi^2} \sin(\omega)$$

$$\xi = \cos(\theta)$$

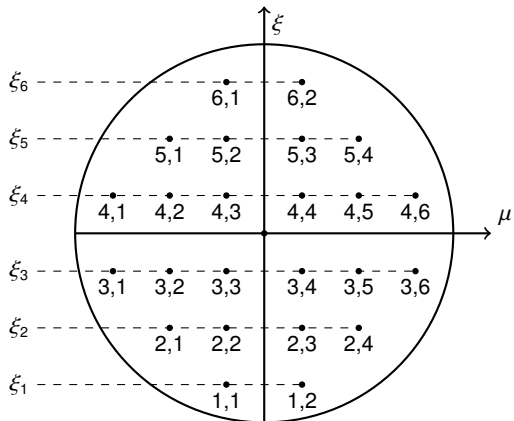
- Direction coordinate axes change with position
- \hat{e}_μ is always in r -direction



R-Z Geometry

Level symmetric angular quadrature

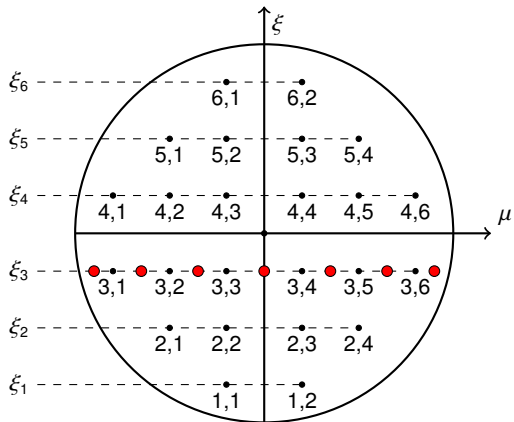
- Angular discretization showing $(\xi_n, \mu_{n,m})$ pairs



R-Z Geometry

Level symmetric angular quadrature

- Angular discretization showing $(\xi_n, \mu_{n,m})$ pairs



R-Z Geometry

Angular derivative approximation - Morel Montry

$$-\frac{1}{r} \frac{\partial}{\partial \omega} \eta \psi(r, z, \Omega) = \frac{\alpha_{m+1/2}^n \psi_{n,m+1/2} - \alpha_{m-1/2}^n \psi_{n,m-1/2}}{r w_{n,m}}$$

R-Z Geometry

Angular derivative approximation - Morel Montry



$$-\frac{1}{r} \frac{\partial}{\partial \omega} \eta \psi(r, z, \Omega) = \frac{\alpha_{m+1/2}^n \psi_{n,m+1/2} - \alpha_{m-1/2}^n \psi_{n,m-1/2}}{r w_{n,m}}$$

- Define angular differencing coefficients to preserve uniform infinite medium solution (i.e., $\Omega \cdot \nabla \psi = 0$)

$$\alpha_{m+1/2}^n = \alpha_{m-1/2}^n - \mu_{n,m} w_{n,m}$$

$$\alpha_{1/2}^n = \alpha_{M_n+1/2}^n = 0$$

R-Z Geometry

Angular derivative approximation - Morel Montry

- Weighted diamond difference approximation for $\psi_{n,m}$ between $\psi_{n,m-1/2}$ and $\psi_{n,m+1/2}$, angular fluxes at the boundary of the discrete ordinate direction

$$\begin{aligned}\psi_{n,m} &= \tau_{n,m}\psi_{n,m+1/2} + (1 - \tau_{n,m})\psi_{n,m-1/2} \\ \tau_{n,m} &= \frac{\mu_{n,m} - \mu_{n,m+1/2}}{\mu_{n,m+1/2} - \mu_{n,m-1/2}}\end{aligned}$$

R-Z Geometry

Angular derivative approximation - Morel Montry

- Weighted diamond difference approximation for $\psi_{n,m}$ between $\psi_{n,m-1/2}$ and $\psi_{n,m+1/2}$, angular fluxes at the boundary of the discrete ordinate direction

$$\psi_{n,m} = \tau_{n,m} \psi_{n,m+1/2} + (1 - \tau_{n,m}) \psi_{n,m-1/2}$$

$$\tau_{n,m} = \frac{\mu_{n,m} - \mu_{n,m+1/2}}{\mu_{n,m+1/2} - \mu_{n,m-1/2}}$$

$$\mu_{n,m+1/2} = \sqrt{1 - \xi_n^2} \cos(\gamma_{n,m+1/2})$$

$$\gamma_{n,m+1/2} = \gamma_{n,m-1/2} + \frac{\pi w_{n,m}}{\sum_{m=1}^{M_n} w_{n,m}}$$

$$\gamma_{n,1/2} = -\pi$$

R-Z Geometry

Angular derivative approximation - Morel Montry

- Solve for starting directions $\psi_{n,1/2}$ using Cartesian geometry transport equation

$$\boldsymbol{\Omega} \cdot \nabla \psi_{n,1/2} + \sigma_t \psi_{n,1/2} = \frac{1}{2\pi} \sigma_s \phi + \frac{1}{2\pi} S_0$$

R-Z Geometry

Angular derivative approximation - Morel Montry

- Solve for starting directions $\psi_{n,1/2}$ using Cartesian geometry transport equation

$$\Omega \cdot \nabla \psi_{n,1/2} + \sigma_t \psi_{n,1/2} = \frac{1}{2\pi} \sigma_s \phi + \frac{1}{2\pi} S_0$$

- Relate the starting direction ($m = 1/2$) to the first discrete ordinates direction ($m = 1$)

$$\psi_{n,1} = \tau_{n,1} \psi_{n,1+1/2} + (1 - \tau_{n,1}) \psi_{n,1/2}$$

R-Z Geometry

Angular derivative approximation - Morel Montry

- Solve for starting directions $\psi_{n,1/2}$ using Cartesian geometry transport equation

$$\boldsymbol{\Omega} \cdot \nabla \psi_{n,1/2} + \sigma_t \psi_{n,1/2} = \frac{1}{2\pi} \sigma_s \phi + \frac{1}{2\pi} S_0$$

- Relate the starting direction ($m = 1/2$) to the first discrete ordinates direction ($m = 1$)

$$\begin{aligned}\psi_{n,1} &= \tau_{n,1} \psi_{n,1+1/2} + (1 - \tau_{n,1}) \psi_{n,1/2} \\ - \frac{1}{r} \frac{\partial}{\partial \omega} \eta \psi &= \frac{\alpha_{1+1/2}^n \psi_{n,1+1/2} - \alpha_{1/2}^n \psi_{n,1/2}}{r w_{n,1}}\end{aligned}$$

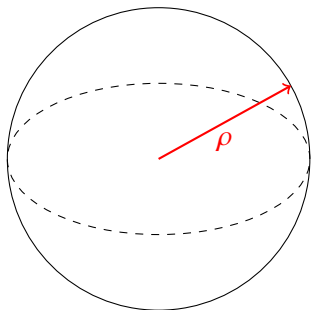


Axisymmetry Preservation

Preserve 1-D spherical symmetry using *R-Z* geometry

- Preserve 1-D spherical symmetry
 - only a function of spherical radius, ρ

$$\rho \equiv \sqrt{r^2 + z^2}$$

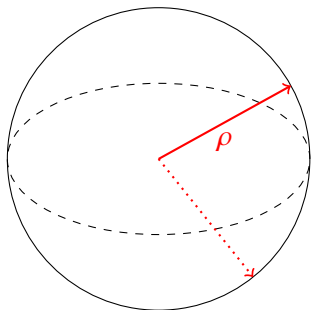


Axisymmetry Preservation

Preserve 1-D spherical symmetry using *R-Z* geometry

- Preserve 1-D spherical symmetry
 - only a function of spherical radius, ρ

$$\rho \equiv \sqrt{r^2 + z^2}$$

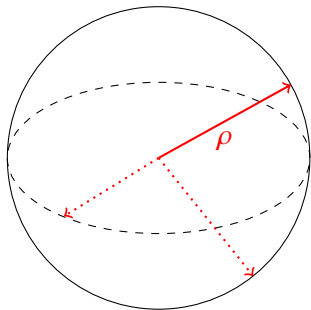


Axisymmetry Preservation

Preserve 1-D spherical symmetry using *R-Z* geometry

- Preserve 1-D spherical symmetry
 - only a function of spherical radius, ρ

$$\rho \equiv \sqrt{r^2 + z^2}$$

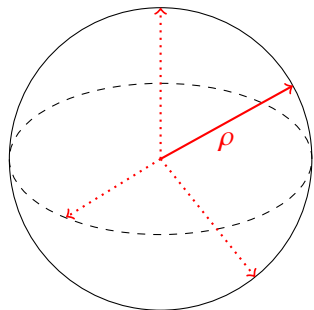


Axisymmetry Preservation

Preserve 1-D spherical symmetry using *R-Z* geometry

- Preserve 1-D spherical symmetry
 - only a function of spherical radius, ρ

$$\rho \equiv \sqrt{r^2 + z^2}$$

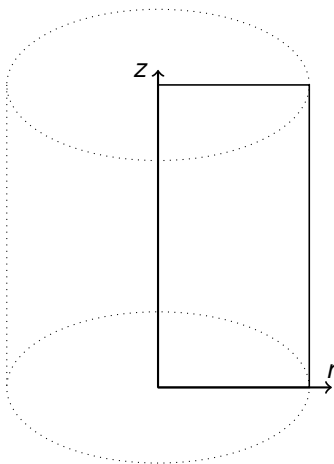
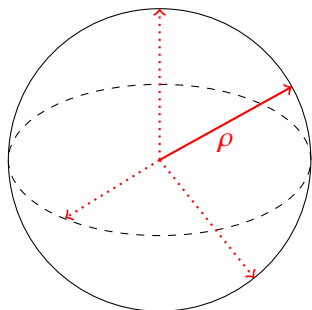


Axisymmetry Preservation

Preserve 1-D spherical symmetry using *R-Z* geometry

- Preserve 1-D spherical symmetry
 - only a function of spherical radius, ρ

$$\rho \equiv \sqrt{r^2 + z^2}$$

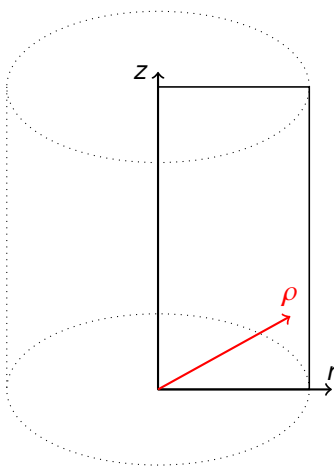
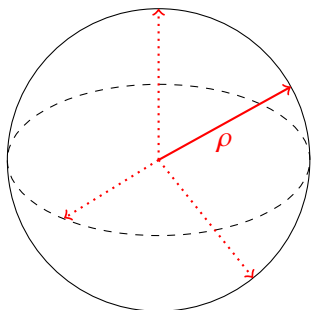


Axisymmetry Preservation

Preserve 1-D spherical symmetry using *R-Z* geometry

- Preserve 1-D spherical symmetry
 - only a function of spherical radius, ρ

$$\rho \equiv \sqrt{r^2 + z^2}$$

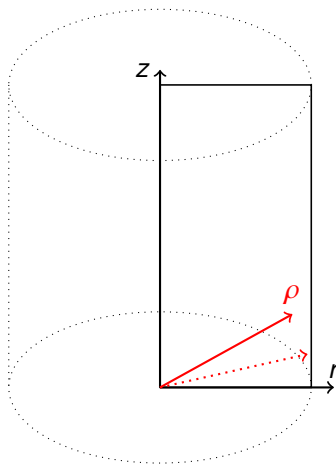
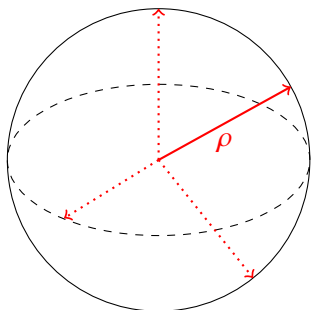


Axisymmetry Preservation

Preserve 1-D spherical symmetry using *R-Z* geometry

- Preserve 1-D spherical symmetry
 - only a function of spherical radius, ρ

$$\rho \equiv \sqrt{r^2 + z^2}$$

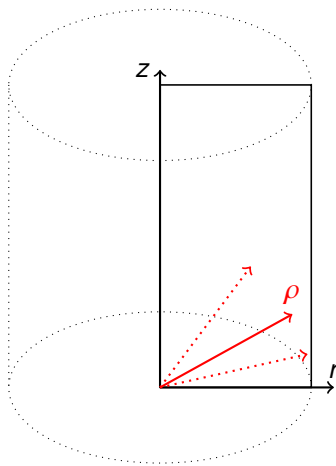
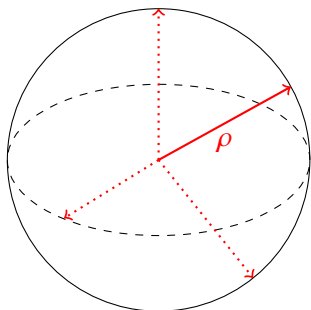


Axisymmetry Preservation

Preserve 1-D spherical symmetry using *R-Z* geometry

- Preserve 1-D spherical symmetry
 - only a function of spherical radius, ρ

$$\rho \equiv \sqrt{r^2 + z^2}$$



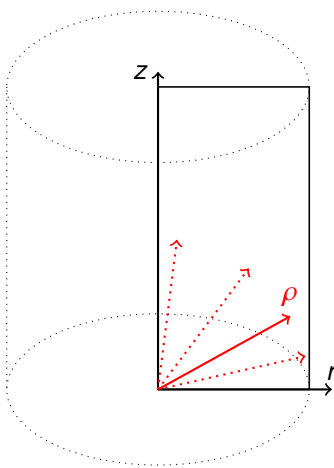
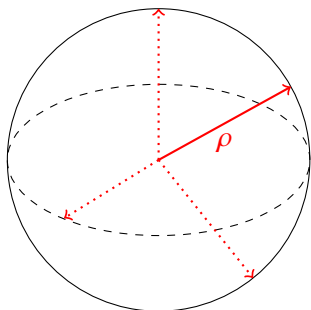
Oregon State
University

Axisymmetry Preservation

Preserve 1-D spherical symmetry using *R-Z* geometry

- Preserve 1-D spherical symmetry
 - only a function of spherical radius, ρ

$$\rho \equiv \sqrt{r^2 + z^2}$$



Axisymmetry Preservation

Preserve 1-D spherical symmetry using *R-Z* geometry

- Solve MMS problem with manufactured solution:

$$\psi_{\text{MMS}} = \rho \equiv \sqrt{r^2 + z^2}$$

- Homogeneous material with $\sigma_t = 5.0$, $\sigma_s = 2.0$
- Incident angular flux on $\rho = 1$ boundary
- Reflecting boundary at $r = 0$
- $p = \{1, 2, 4, 8\}$, several S_N orders ($N = \{4, 6, 8, 10, 12\}$), 1st- and 2nd-order meshes, several mesh refinements

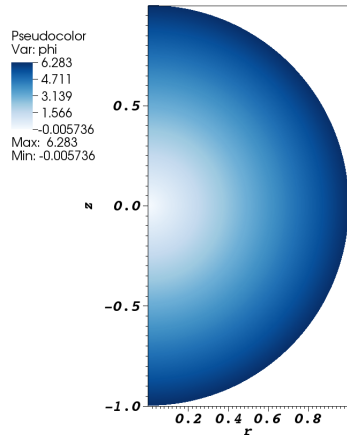
Axisymmetry Preservation

Preserve 1-D spherical symmetry using *R-Z* geometry

- Solve MMS problem with manufactured solution:

$$\psi_{\text{MMS}} = \rho \equiv \sqrt{r^2 + z^2}$$

- Homogeneous material with $\sigma_t = 5.0, \sigma_s = 2.0$
- Incident angular flux on $\rho = 1$ boundary
- Reflecting boundary at $r = 0$
- $p = \{1, 2, 4, 8\}$, several S_N orders ($N = \{4, 6, 8, 10, 12\}$), 1st- and 2nd-order meshes, several mesh refinements



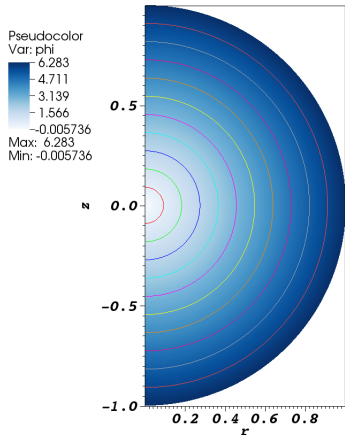
Axisymmetry Preservation

Preserve 1-D spherical symmetry using R - Z geometry

- Solve MMS problem with manufactured solution:

$$\psi_{\text{MMS}} = \rho \equiv \sqrt{r^2 + z^2}$$

- Homogeneous material with $\sigma_t = 5.0$, $\sigma_s = 2.0$
- Incident angular flux on $\rho = 1$ boundary
- Reflecting boundary at $r = 0$
- $p = \{1, 2, 4, 8\}$, several S_N orders ($N = \{4, 6, 8, 10, 12\}$), 1st- and 2nd-order meshes, several mesh refinements



Axisymmetry Preservation

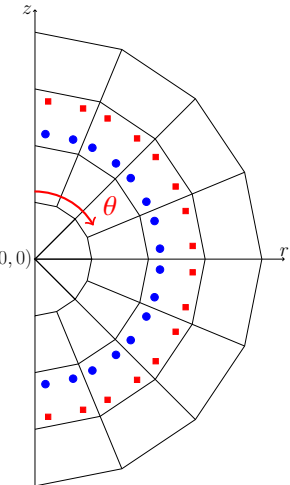
Preserve 1-D spherical symmetry using *R-Z* geometry

- Compare each nodal solution to the average solution at each spherical radius
 $\rho = \sqrt{r^2 + z^2}$

$$\phi_{\text{asym}}(\rho) = \left| \frac{\phi_{\text{DFEM}}(\rho, \theta) - \phi_{\text{avg}}(\rho)}{\phi_{\text{avg}}(\rho)} \right|$$

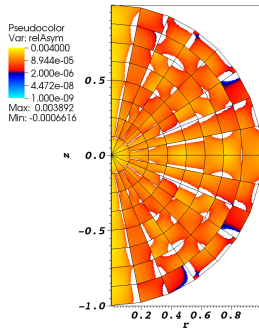
$$\phi_{\text{avg}}(\rho) = \frac{1}{N_{\text{nodes}}(\rho)} \sum_{i=1}^{N_{\text{nodes}}(\rho)} \phi_{\text{DFEM}}(\rho, \theta_i)$$

- Plot the FEM “shape” of ϕ_{asym}

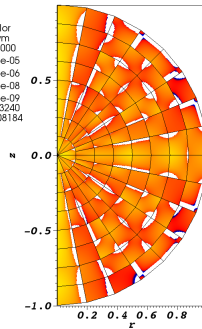


Axisymmetry Preservation

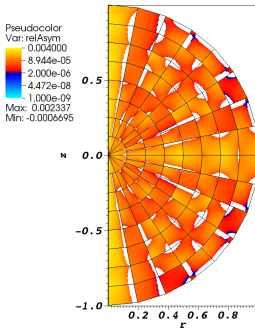
Relative asymmetry for 1st-order finite elements on a 1st-order mesh for given order of level-symmetric angular quadrature



(a) S_4



(b) S_8

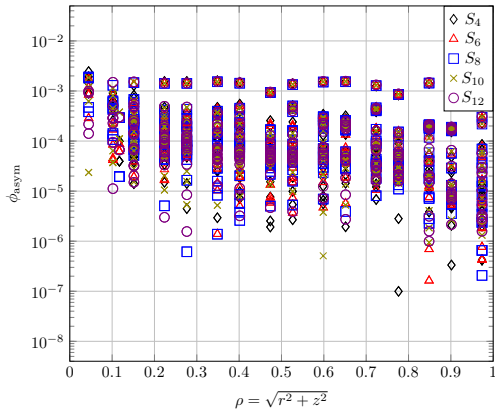


(c) S_{12}

Axisymmetry Preservation

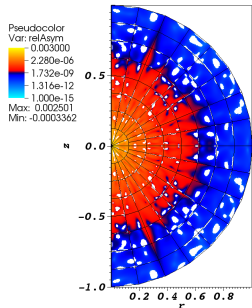
Relative asymmetry for 1st-order finite elements on a 1st-order mesh for given order of level-symmetric angular quadrature

- Difficult to distinguish between S_N solutions
- Greatest asymmetry near origin
- Asymmetry reaches an asymptotic value $\sim 10^{-3}$
- Accuracy of solution is nearly constant

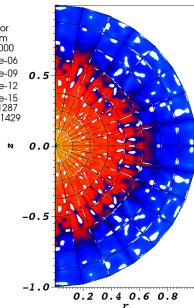


Axisymmetry Preservation

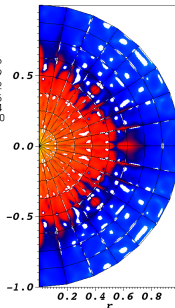
Relative asymmetry for 4th-order finite elements on a 1st-order mesh for given order of level-symmetric angular quadrature



(a) S_4



(b) S_8

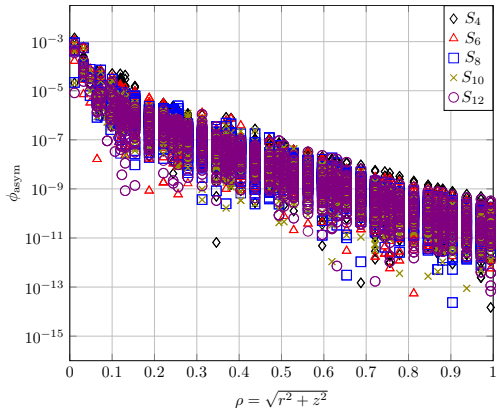


(c) S_{12}

Axisymmetry Preservation

Relative asymmetry for 4th-order finite elements on a 1st-order mesh for given order of level-symmetric angular quadrature

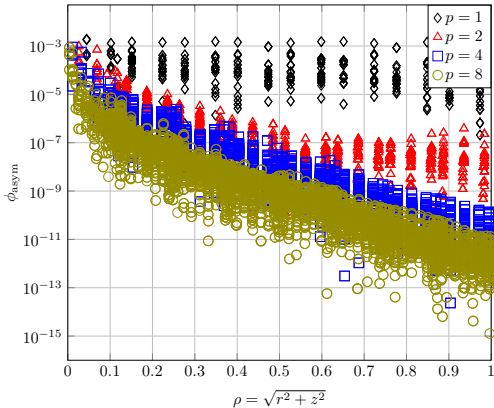
- Difficult to distinguish between S_N solutions
- Greatest asymmetry near origin
- Asymmetry does not reach an asymptotic value ($< 10^{-9}$)
- Accuracy of solution is nearly constant



Axisymmetry Preservation

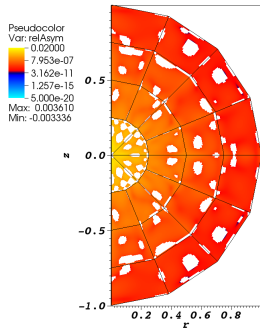
Relative asymmetries for each finite element order on a 1st-order mesh for S_8 level-symmetric angular quadrature

- 1st- and 2nd-order finite elements reach asymptotic asymmetry
- Increasing finite element order increases relative symmetry
- Asymmetry does not reach an asymptotic value ($< 10^{-9}$) for higher-order finite elements
- Relative symmetry is nearly identical at the origin

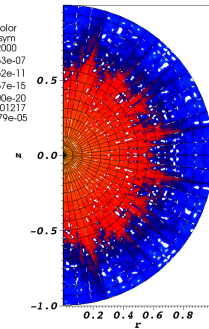


Axisymmetry Preservation

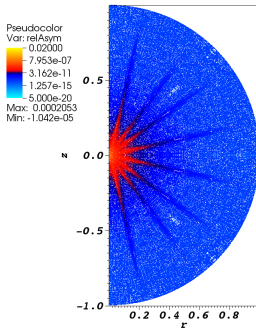
Relative asymmetry under spatial refinement for 4th-order finite elements on a 1st-order mesh for given order of level-symmetric angular quadrature



(a) 28 zones



(b) 496 zones

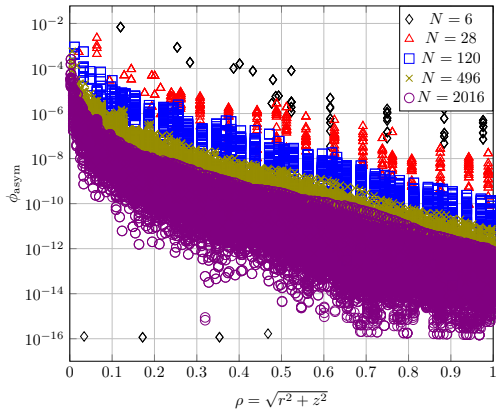


(c) 8128 zones

Axisymmetry Preservation

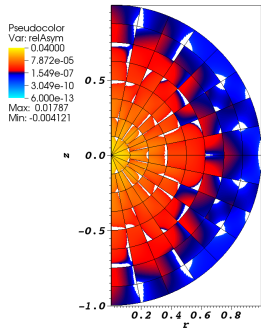
Relative asymmetries under spatial refinement for 4st-order finite elements on a 1st-order mesh for S_8 level-symmetric angular quadrature

- Mesh refinement increases symmetry preservation
- Largest magnitude asymmetries are located near the origin
- Mesh refinement increases accuracy of scalar flux

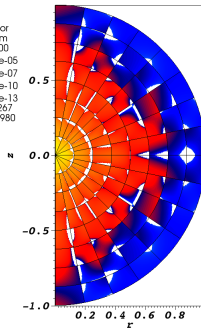


Axisymmetry Preservation

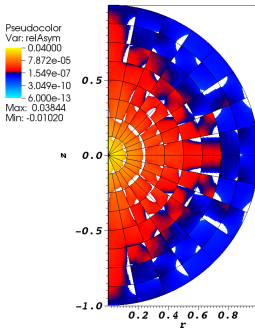
Relative asymmetry for 1st-order finite elements on a 2nd-order mesh for given order of level-symmetric angular quadrature



(a) S_4



(b) S_8

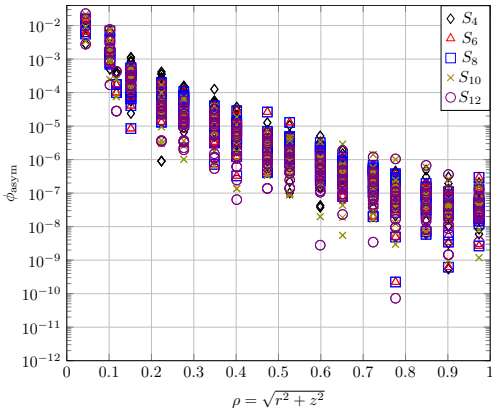


(c) S_{12}

Axisymmetry Preservation

Relative asymmetry for 1st-order finite elements on a 2nd-order mesh for given order of level-symmetric angular quadrature

- Difficult to distinguish between S_N solutions
- Greatest asymmetry near origin
- Asymmetry does not reach an asymptotic value ($< 10^{-6}$)
- Accuracy is nearly constant



R-Z Geometry Conclusions

- Implemented and characterized the *R-Z* spatial discretization using HO finite elements on meshes with curved surfaces
- Axisymmetry preservation is conditional with two dominant factors:
 - spatial mesh refinement
 - finite element order
- Future work
 - Numerically demonstrate diffusion limit
 - Consider alternate derivations of *R-Z* equations
 - Consider other manufactured solutions and materials for symmetry preservation



MIP DSA Conclusions

- Implemented MIP DSA equations with Robin boundary conditions
 - Unconditionally converging (i.e. $\rho < 1$)
 - Greatly accelerates source iteration
- Compared spectral radii to the MIP DSA equations with Dirichlet boundary conditions
 - Robin BCs do not generate the peaks
 - Robin BCs are not as dependent on the constant C or ρ
 - Robin BCs have significantly higher spectral radii in optically thick region
- Future work
 - Investigate the optically thick region
 - Fourier analysis

Thank you!



Oregon State
University

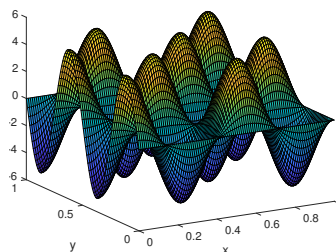
X-Y Geometry

Spatial convergence study

- Method of manufactured solutions (MMS) to determine convergence rates

$$\psi_{\text{MMS}} = (1 - \mu^2)(1 - \eta^2) \sin(4\pi x) \cos\left(\frac{7}{2}\pi y\right)$$

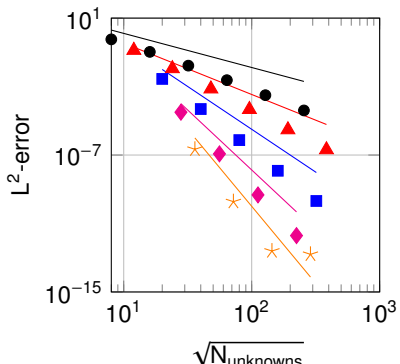
- Calculate $\|\phi_{\text{code}} - \phi_{\text{MMS}}\|_{L^2}$ for sequential mesh refinements
- Use $p = \{1, 2, 4, 6, 8\}$
- Orthogonal and 3rd-order meshes



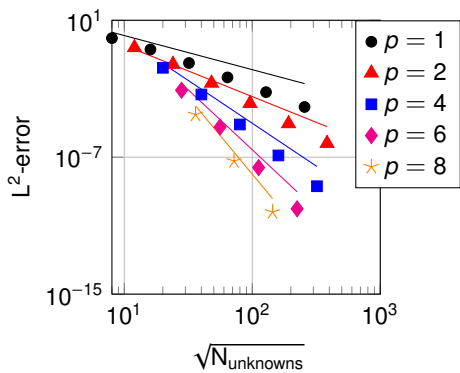
X-Y Geometry

Spatial convergence study shows $p + 1$ convergence

- $N_{\text{unknowns}} = N_{\text{cells}}(p + 1)^2$
- Reference lines show $p + 1$ spatial convergences



Orthogonal mesh



3rd-order mesh



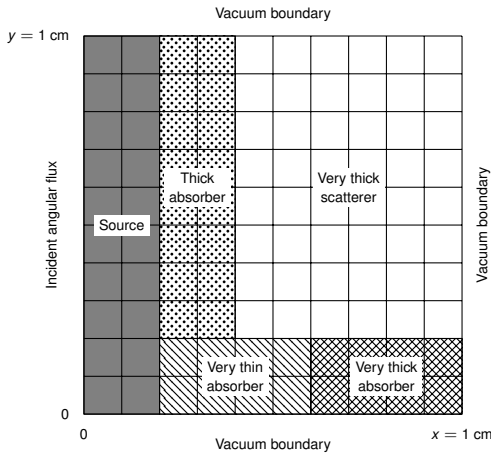
Oregon State
University

X-Y Geometry

Strong material heterogeneity problem definition

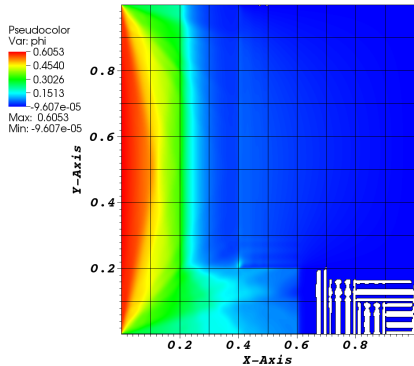
Material Region	$\sigma_t \text{ cm}^{-1}$	$\sigma_s \text{ cm}^{-1}$
Source	1.0	1.0
Very thin absorber	0.0001	0.0
Thick absorber	10.0	0.0
Very thick absorber	100.0	0.0
Very thick scatterer	1000.0	1000.0

- Designed to test optical thicknesses ranging several orders of magnitude
- Create anisotropic fluxes into scattering region

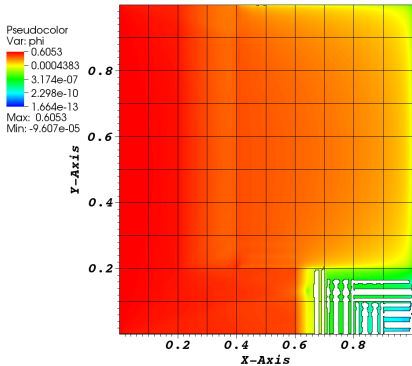


X-Y Geometry

Strong material heterogeneity problem results



Multi-material stress test solved with Robin BC MIP DSA. White regions indicate negative energy density.



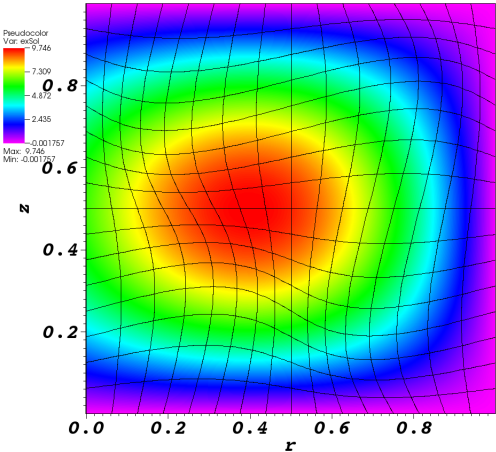
Log of multi-material stress test solved with Robin BC MIP DSA. White regions indicate negative energy density.

R-Z Geometry

MMS spatial convergence study

$$\psi_{\text{MMS}} = (\sin(\pi r) + 1 - r) \sin(\pi z)$$

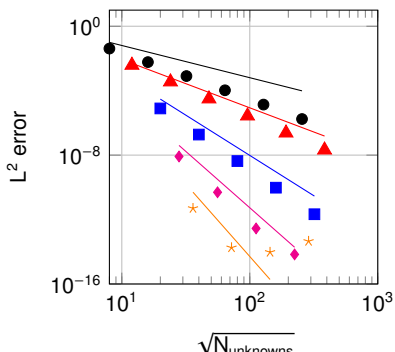
- Bailey et al. demonstrated 2nd-order convergence for PWL and BLD
- We solve using $p = \{1, 2, 4, 6, 8\}$ on an orthogonal and 2nd-order curved mesh
- S_8 level-symmetric angular quadrature



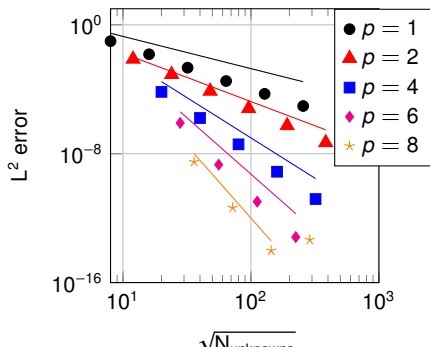
R-Z Geometry

MMS spatial convergence study shows $p + 1$ convergence

- $N_{\text{unknowns}} = N_{\text{cells}}(p + 1)^2$
- Reference lines show $p + 1$ spatial convergences



Orthogonal mesh



2nd-order curved mesh

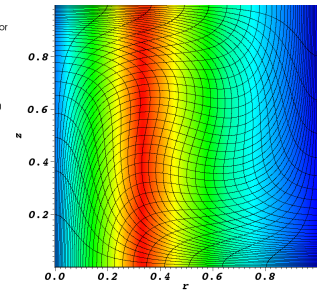
R-Z Geometry

Regularity constrained spatial convergence study shows $O(3/2)$ convergence rates

- Method of manufactured solutions (MMS) to determine convergence rates

$$\psi_{\text{MMS}} = \begin{cases} 1.0 + 4.0r, & 0 \leq r < 0.33 \\ 3.31 - 3.0r, & 0.33 \leq r < 0.66 \\ 2.32 - 1.5r, & r \leq 1.0 \end{cases}$$

- Calculate $\|\phi_{\text{code}} - \phi_{\text{MMS}}\|_{L^2}$ for sequential mesh refinements
- Use $p = \{1, 2, 4\}$, S_{12} level-symmetric angular quadrature, 2nd-order mesh



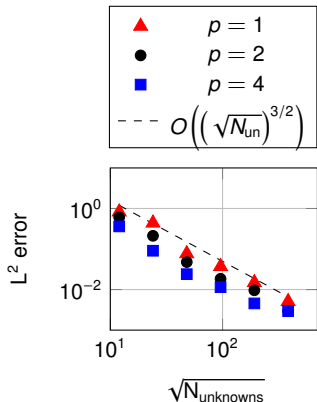
R-Z Geometry

Regularity constrained spatial convergence study shows $O(3/2)$ convergence rates

- Method of manufactured solutions (MMS) to determine convergence rates

$$\psi_{\text{MMS}} = \begin{cases} 1.0 + 4.0r, & 0 \leq r < 0.33 \\ 3.31 - 3.0r, & 0.33 \leq r < 0.66 \\ 2.32 - 1.5r, & r \leq 1.0 \end{cases}$$

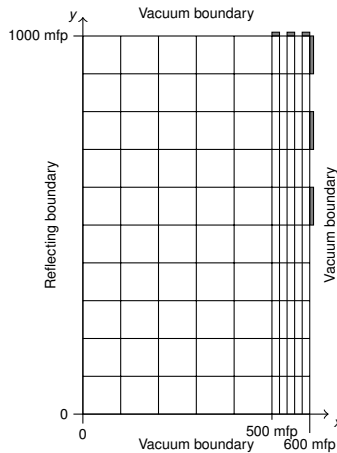
- Calculate $\|\phi_{\text{code}} - \phi_{\text{MMS}}\|_{L^2}$ for sequential mesh refinements
- Use $p = \{1, 2, 4\}$, S_{12} level-symmetric angular quadrature, 2nd-order mesh



R-Z Geometry

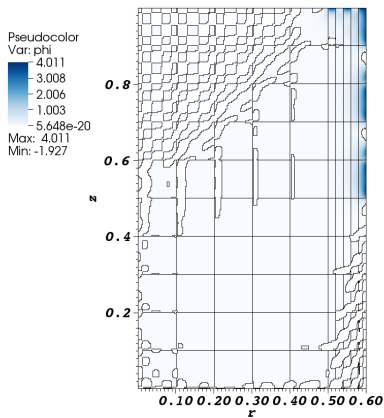
Strong scatter with alternating boundary conditions

- Incident flux boundary at gray cells
 $\psi_{\text{inc}} = 2/\pi$
- $\sigma_t = 1000, \sigma_s = 999, S_0 = 0$
- 4th-order finite elements
- Designed to reveal boundary layer

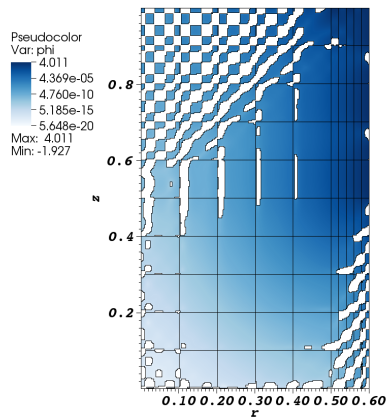


R-Z Geometry

Strong scatter with alternating boundary conditions



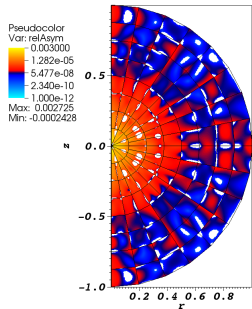
Scalar flux; white regions indicate negative scalar flux.



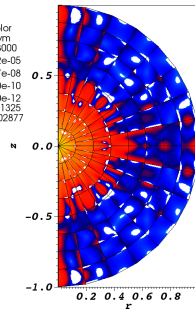
Log of scalar flux; white regions indicate negative scalar flux.

Axisymmetry Preservation

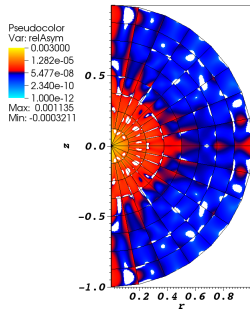
Relative asymmetry for 2nd-order finite elements on a 1st-order mesh for given order of level-symmetric angular quadrature



(a) S_4



(b) S_8

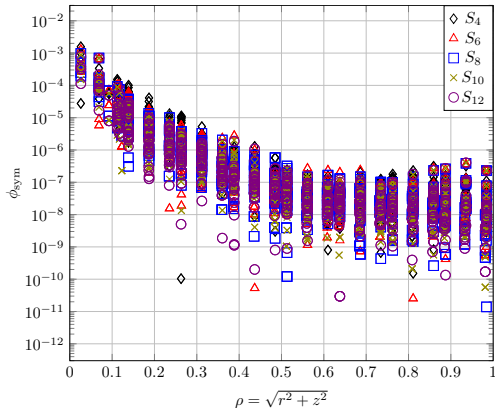


(c) S_{12}

Axisymmetry Preservation

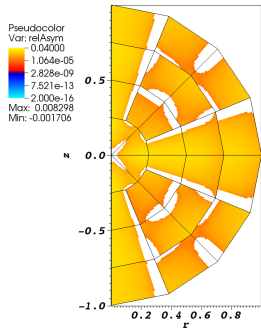
Relative asymmetry for 2nd-order finite elements on a 1st-order mesh for given order of level-symmetric angular quadrature

- Difficult to distinguish between S_N solutions
- Greatest asymmetry near origin
- Asymmetry reaches an asymptotic value $\sim 10^{-7}$
- Accuracy of solution is nearly constant

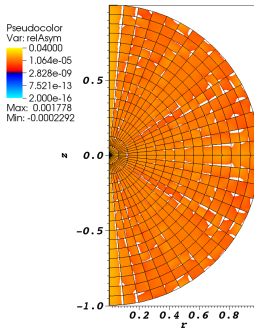


Axisymmetry Preservation

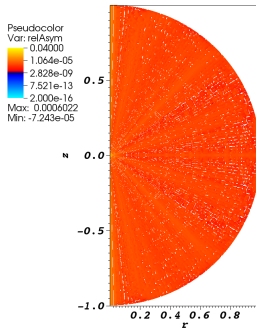
Relative asymmetry under spatial refinement for 1st-order finite elements on a 1st-order mesh for given order of level-symmetric angular quadrature



(a) 28 zones



(b) 496 zones

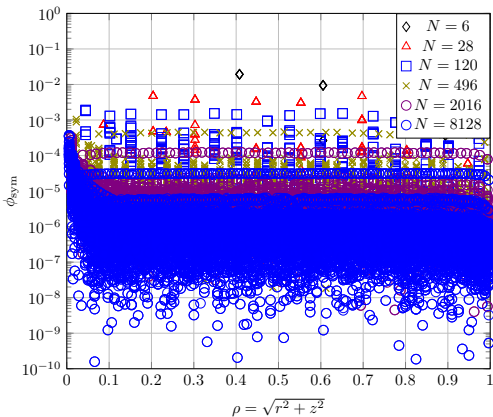


(c) 8128 zones

Axisymmetry Preservation

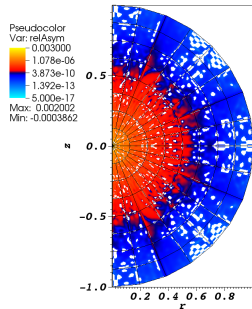
Relative asymmetries under spatial refinement for 1st-order finite elements on a 1st-order mesh for S_8 level-symmetric angular quadrature

- Spatial refinement increases the symmetry preservation
- Bands appear from nodes near the z-axis
- Largest magnitude asymmetries are located near the origin

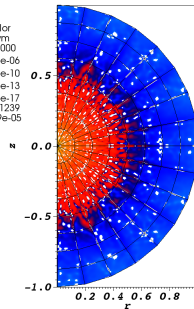


Axisymmetry Preservation

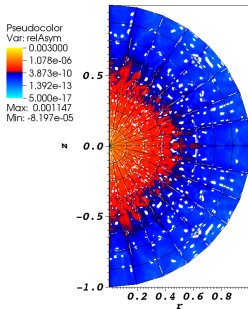
Relative asymmetry for 8th-order finite elements on a 1st-order mesh for given order of level-symmetric angular quadrature



(a) S_4



(b) S_8

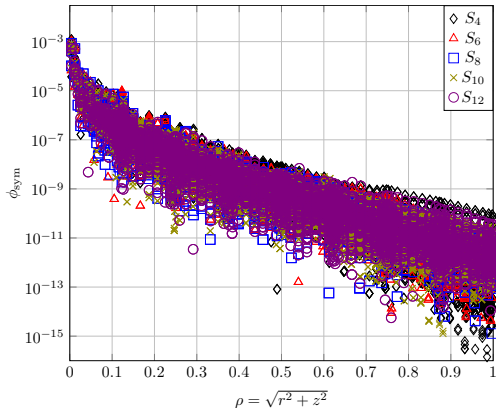


(c) S_{12}

Axisymmetry Preservation

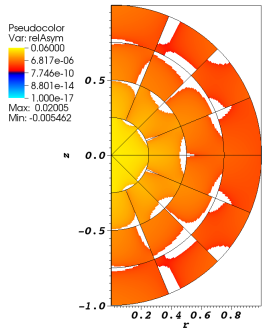
Relative asymmetry for 8th-order finite elements on a 1st-order mesh for given order of level-symmetric angular quadrature

- Difficult to distinguish between S_N solutions
- Greatest asymmetry near origin
- Asymmetry does not reach an asymptotic value ($< 10^{-10}$)
- Not a tremendous gain in symmetry compared to 4th-order finite elements
- Accuracy of solution is nearly constant

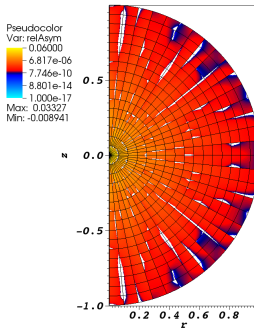


Axisymmetry Preservation

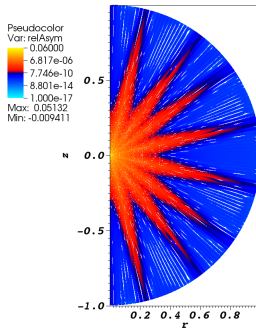
Relative asymmetry under spatial refinement for 1st-order finite elements on a 2nd-order mesh for given order of level-symmetric angular quadrature



(a) 28 zones



(b) 496 zones

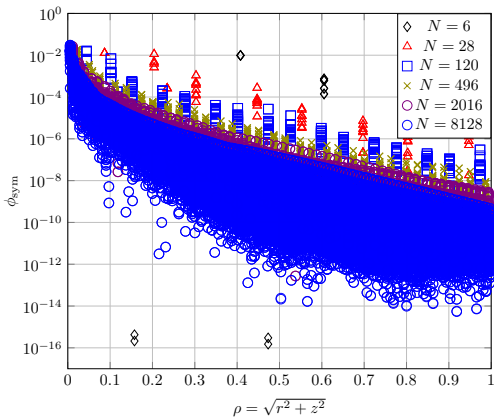


(c) 8128 zones

Axisymmetry Preservation

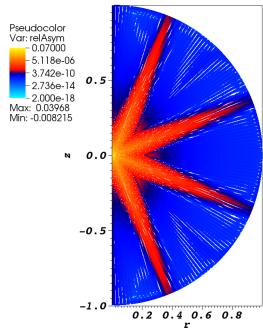
Relative asymmetries under spatial refinement for 1st-order finite elements on a 2nd-order mesh for S_8 level-symmetric angular quadrature

- Spatial refinement increases the symmetry preservation
- Apparent “ray-effects”
- Largest magnitude asymmetries are located near the origin

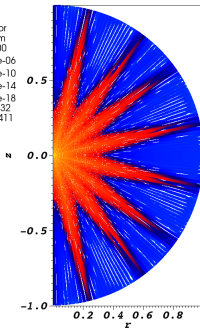


Axisymmetry Preservation

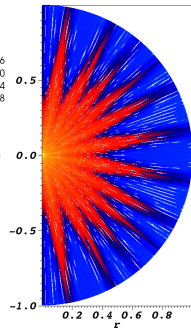
Relative asymmetry under spatial refinement for 1st-order finite elements on a 2nd-order mesh



(a) S_4



(b) S_8

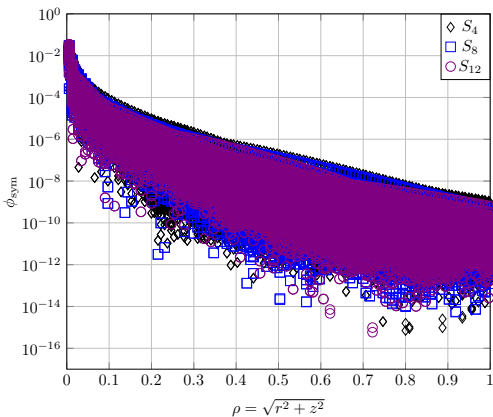


(c) S_{12}

Axisymmetry Preservation

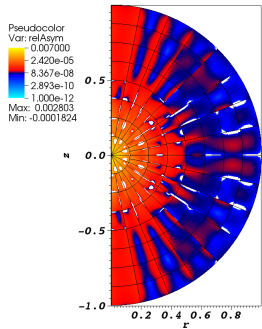
Relative asymmetries under spatial refinement for 1nd-order finite elements on a 2nd-order mesh for given level-symmetric angular quadrature

- Mesh refinement increases symmetry preservation
- Largest magnitude asymmetries are located near the origin

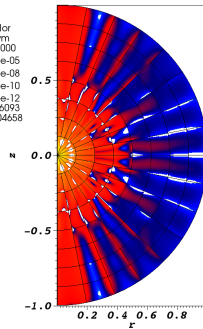


Axisymmetry Preservation

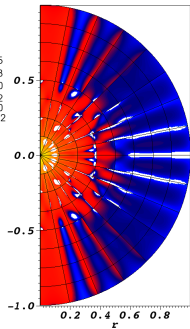
Relative asymmetry for 2nd-order finite elements on a 2nd-order mesh for given order of level-symmetric angular quadrature



(a) S_4



(b) S_8

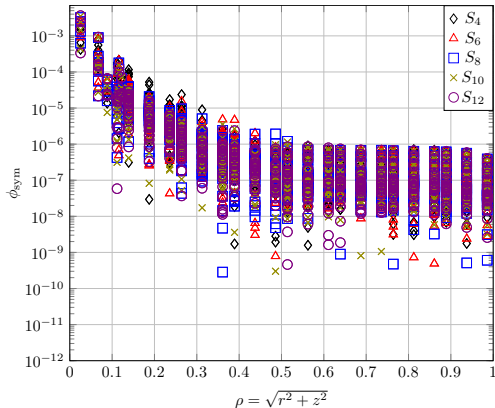


(c) S_{12}

Axisymmetry Preservation

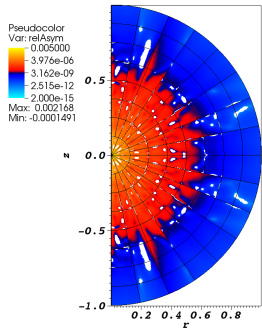
Relative asymmetry for 2nd-order finite elements on a 2nd-order mesh for given order of level-symmetric angular quadrature

- Difficult to distinguish between S_N solutions
- Greatest asymmetry near origin
- Large asymmetry on z-axis
- Asymmetry reaches an asymptotic value $\sim 10^{-6}$
- Accuracy is nearly constant

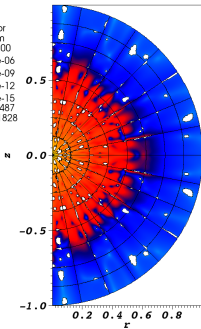


Axisymmetry Preservation

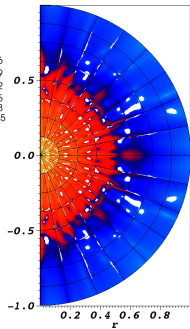
Relative asymmetry for 4th-order finite elements on a 2nd-order mesh for given order of level-symmetric angular quadrature



(a) S_4



(b) S_8

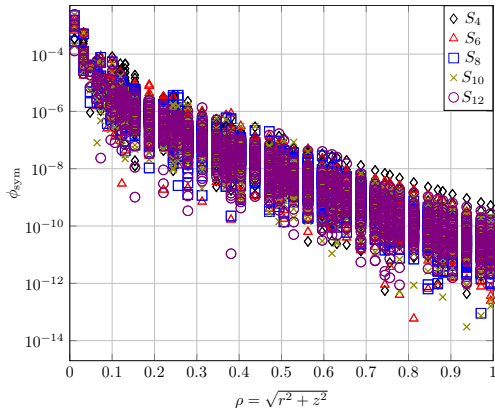


(c) S_{12}

Axisymmetry Preservation

Relative asymmetry for 4th-order finite elements on a 2nd-order mesh for given order of level-symmetric angular quadrature

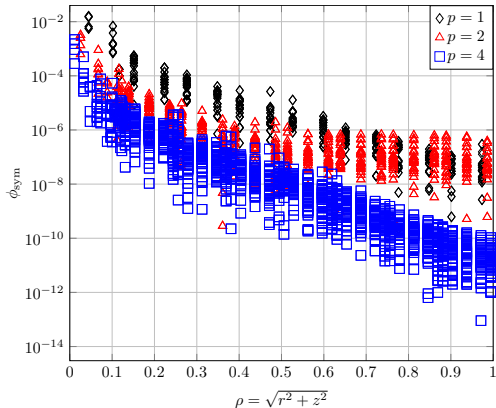
- Difficult to distinguish between S_N solutions
- Greatest asymmetry near origin
- Asymmetry does not reach an asymptotic value ($< 10^{-9}$)



Axisymmetry Preservation

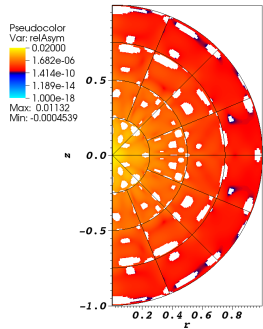
Relative asymmetries for each finite element order on a 2nd-order mesh for S_8 level-symmetric angular quadrature

- 2nd-order finite elements reach a larger asymptotic asymmetry value
- Increasing finite element order increases relative symmetry
- Relative symmetry is similar at the origin

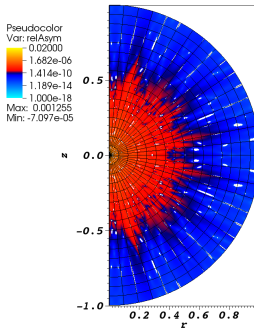


Axisymmetry Preservation

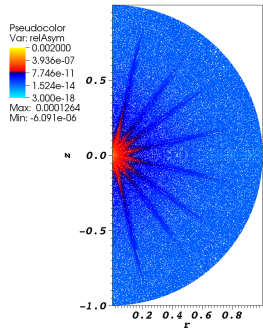
Relative asymmetry under spatial refinement for 4th-order finite elements on a 2nd-order mesh for given order of level-symmetric angular quadrature



(a) 28 zones



(b) 496 zones

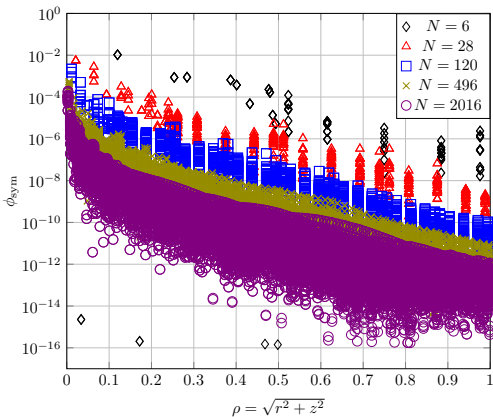


(c) 8128 zones

Axisymmetry Preservation

Relative asymmetries under spatial refinement for 4st-order finite elements on a 2nd-order mesh for S_8 level-symmetric angular quadrature

- Mesh refinement increases symmetry preservation
- Largest magnitude asymmetries are located near the origin



Axysmmetry Preservation

MMS solution has strong gradient near the origin

$$\psi_{\text{MMS}}(r, z) = \rho$$

$$\equiv \sqrt{r^2 + z^2}$$

